



OPEN ACCESS

EDITED BY

A. Menchaca,
Fundacion IRAUy, Uruguay

REVIEWED BY

Ashik Banstola,
University of Otago, New Zealand
Mizael Machado,
National Institute for Agricultural Research
(INIA), Uruguay
Julián Yáñez,
University of A Coruña, Spain

*CORRESPONDENCE

Miguel Merchán Jr.
✉ miguelml@usal.es
Carlos Palacios
✉ carlospalacios@usal.es

SPECIALTY SECTION

This article was submitted to
Animal Reproduction - Theriogenology,
a section of the journal
Frontiers in Veterinary Science

RECEIVED 17 November 2022

ACCEPTED 31 January 2023

PUBLISHED 16 February 2023

CITATION

Merchán M Jr, Coveñas R, Plaza I, Abecia JA
and Palacios C (2023) Anatomy of
hypothalamic and diencephalic nuclei involved
in seasonal fertility regulation in ewes.
Front. Vet. Sci. 10:1101024.
doi: 10.3389/fvets.2023.1101024

COPYRIGHT

© 2023 Merchán, Coveñas, Plaza, Abecia and
Palacios. This is an open-access article
distributed under the terms of the [Creative
Commons Attribution License \(CC BY\)](#). The use,
distribution or reproduction in other forums is
permitted, provided the original author(s) and
the copyright owner(s) are credited and that
the original publication in this journal is cited, in
accordance with accepted academic practice.
No use, distribution or reproduction is
permitted which does not comply with these
terms.

Anatomy of hypothalamic and diencephalic nuclei involved in seasonal fertility regulation in ewes

Miguel Merchán Jr.^{1,2,3*}, Rafael Coveñas^{2,3}, Ignacio Plaza⁴,
José Alfonso Abecia⁵ and Carlos Palacios^{1*}

¹Animal Production Area, Department of Construction and Agronomy, Faculty of Agricultural and Environmental Sciences, University of Salamanca, Salamanca, Spain, ²Laboratory of Neuroanatomy of the Peptidergic Systems, Institute for Neuroscience of Castilla y León (INCYL), University of Salamanca, Salamanca, Spain, ³Recognized Research Group - Molecular Bases of Development (Grupo de Investigación Reconocido - Bases Moleculares del Desarrollo - GIR-BMD), University of Salamanca, Salamanca, Spain, ⁴Auditory Neuroplasticity Laboratory, Institute for Neuroscience of Castilla y León (INCYL), University of Salamanca, Salamanca, Spain, ⁵Environmental Science Institute (IUCA), University of Zaragoza, Zaragoza, Spain

In this study, we describe in detail the anatomy of nuclei involved in seasonal fertility regulation (SFR) in ewes. For this purpose, the intergeniculate leaflet of the visual thalamus, the caudal hypothalamic arcuate nucleus, and suprachiasmatic, paraventricular and supraoptic nuclei of the rostral hypothalamus were morphometrically and qualitatively analyzed in Nissl-stained serial sections, in the three anatomical planes. In addition, data were collected on calcium-binding proteins and cell phenotypes after immunostaining alternate serial sections for calretinin, parvalbumin and calbindin. For a complete neuroanatomical study, glial architecture was assessed by immunostaining and analyzing alternate sections for glial fibrillary acidic protein (GFAP) and ionized calcium-binding adapter molecule 1 (IBA1). The results showed a strong microglial and astroglia reaction around the hypothalamic nuclei of interest and around the whole 3rd ventricle of the ewe brain. Moreover, we correlated cytoarchitectonic coordinates of panoramic serial sections with their macroscopic localization and extension in midline sagittal-sectioned whole brain to provide guidelines for microdissecting nuclei involved in SFR.

KEYWORDS

calbindin, calretinin, parvalbumin, GFAP, IBA1, Nissl staining

1. Introduction

Sheep are ruminants and seasonal breeders. As a result, sheep farming is misaligned with market demands (e.g., continuous production throughout the year), and the income derived from these seasonal animals is lower than that derived from non-seasonal animals (1). For this reason, one of the most important goals for seasonal animal husbandry (e.g., sheep) is to achieve continuous production throughout the year by shortening the periods between lambing, thereby improving production rates (2, 3).

Seasonality, an adaptive process whereby animals adapt their physiological functions (e.g., reproduction) to the environmental conditions (4), has been studied in several species ranging from invertebrates to vertebrates (5–7). In particular, research has focused on understanding the neurological basis of seasonal breeding among farm animals (e.g., sheep and goats) (8–10). Thus, structural plasticity changes, cell proliferation and migration in the sheep hypothalamus indicate that seasonal light changes induce a deep neural reorganization

(11–13). Furthermore, recent studies have shown that polymorphisms in genes encoding melatonin 1A and 1B receptors (*MTNR1A* and *MTNR1B*, respectively) are involved in reproductive seasonality (14–17). Concurrently, anatomical and physiological studies have implicated melatonin in the control of seasonal breeding or estrous cyclicity (18, 19). Based on these findings, attempts have been made to regulate the circadian cycle of sheep by changing their natural photoperiod in combination with melatonin implants and hormone treatments (20–22).

In immunohistochemical studies, kisspeptin, neurokinin A and dynorphin B, called KNDy neurons, and Gonadotropin Releasing hormone (GnRH) neurons have also been identified in the sheep hypothalamus, highlighting their key role in the endocrine regulation of seasonal breeding (8, 23–25). However, analyzing interactions and the complex neuronal machinery involved in the hypothalamic regulation of seasonality requires understanding its neuroanatomical underpinnings. The main nuclei involved in circadian rhythm regulation in rodents and non-human primates are the hypothalamic suprachiasmatic nucleus (SCh) and the diencephalic intergeniculate leaflet (IGL) nucleus of the thalamus (26). Other hypothalamic nuclei also involved in seasonality include the supraoptic (SO), paraventricular (PVN) and arcuate (ARC) nuclei (27, 28). With slight differences in morphology and spacial distribution, these nuclei are present in all higher mammals, including sheep (11, 26, 29–31). Full neuroanatomical and neurochemical studies of hypothalamic nuclei involved in seasonal regulation (e.g., circadian rhythms and seasonal changes in GnRH regulation) must be conducted to gain further insights into the neural basis of fertility regulation in sheep (24, 32, 33).

A few anatomical atlases of the ruminant brain (e.g., sheep, goat, and alpaca) have been previously published (34–37). These studies have used a wide range of methods, including gross anatomy, high-resolution 3D Magnetic Resonance Imaging, and immunohistochemistry or Nissl-stained sections. A highly detailed general description of sheep diencephalic nuclei was reported in a doctoral dissertation dating back to 1976, using coronal thionine-stained serial sections (38) however it was not interpreted in the context of the neuromeric model. Thus, further research should be conducted to analyze in detail the sheep neuroanatomical structures involved in seasonal breeding.

In this article, we describe the anatomical analysis of SFR nuclei using Nissl-stained serial sections and immunocytochemistry for

CBPs. For this purpose, we selected three CBPs, namely Cr, Cb and PV, which have been widely used as markers for cytoarchitectural analysis and for neuronal phenotyping in different vertebrate species (39, 40).

Considering the above, the present study aimed at, (1) determining the morphological features and relative position (coordinates) of seasonal fertility regulation (SFR) nuclei in the ewe diencephalon and hypothalamus by analyzing Nissl-stained serial sections in the three anatomical planes based on high-resolution panoramic photographs, (2) studying the immunohistochemical calbindin (Cb), calretinin (Cr) and parvalbumin (Pv) profile of SFR nuclei, (3) analyzing the morphology, distribution, and cell density gradients (glial architecture) of microglial and astroglia cells in the ewe hypothalamus, and (4) generating a macroscopic map with the specific coordinates and extension of SFR nuclei to enable their accurate localization for microdissections.

2. Materials and methods

2.1. Experimental groups

Six adults female Churra sheep (age = 16.60 ± 0.25 months); mean live weight [(LW) = 70 ± 6 kg] housed under natural light, temperature, and humidity conditions, fed *ad libitum* and provided with unrestricted access to clean drinking water, were used in this study over farm natural conditions. The experiments were performed in accordance with Spanish (RD 53/2013) and European (63/2010/EU) directives, and animal maintenance and care met all requirements of the agreement on the use of animals in scientific experimentation in Spain (Confederation of Scientific Societies of Spain - COSCE). Accordingly, the animals were sacrificed at the slaughterhouse MACRISA, in Medina de Rioseco, Valladolid, Spain, in April 2021, by neck cutting, severing the carotid and jugular veins, without prior drug administration. Heparinized 5-ml tubes were used to collect blood samples by jugular venipuncture; samples were immediately centrifugated at 3000 × g for 20 min, and plasma was stored at −20°C. Hormonal levels of progesterone were assayed by radioimmunoassay (RIA). All samples were run in a single assay. In all specimens, the progesterone levels were homogeneous, ranging from 15 to 20 mg/l.

2.2. Animal samples

After removing the skin, a horizontal cut was made in the skull from the external occipital protuberance to the upper edges of the orbits using an ultra-fast surgical saw with a 5 cm diameter radial disc. Using this approach, the dorsal superficial area of the cortex was cleanly cut, thus showing in depth the ventricles in the middle line maintaining intact the diencephalic area. This procedure provided access to the ventricles for a faster and more effective fixation. After tilting the skull backwards with a spatula and a pair of tweezers, the brain was gently pushed to ventrally cut the optic nerves to rostrally free the brain and to reveal and cut the pituitary stem. Caudally cranial nerves and meningeal flanges were severed. As a result, the brains shed and fell off under their own weight. The nerves were cut with a vise, and the meninges

Abbreviations: AHy, Anterior Hypothalamic area; ARC, Arcuate nucleus; CBPs- Calcium binding protein; Cb, Calbindin; Ci, Capsula interna; Cr, Calretinin; GFAP, glial fibrillary acidic protein; GP, Globus pallidus; GnRH, Gonadotropin Releasing hormone; IBA1, ionized calcium-binding adapter molecule 1; IGL, Intergeniculate leaflet; Inf, infundibulum; KNDy, kisspeptin, neurokinin A and dynorphin B neurons; LG, lateral geniculate nucleus; LPO, Lateral preoptic area; MB, mammillary bodie; ME, median eminence; MPO, Medial preoptic area; mt, mamillothalamic tract; ON, Optic nerve; OT, Optic tract; OX, Optic chiasma; Pi, Pineal gland; POA, Preoptic area; PGN, pregeniculate nucleus; Pv, Parvalbumin; PVN, Paraventricular nucleus; PHYP, peduncular hypothalamus; SCh, Suprachiasmatic nucleus; SFR, Seasonal fertility regulation; SO, Supraoptic nucleus; Thy0- Terminal hypothalamus; VMH, Ventromedial hypothalamus nucleus; IIIV – third ventricle; SFR, Seasonal fertility regulation.

were removed from the pituitary stalk to facilitate infiltration of the fixative solution. The time elapsed from euthanasia to brain and pituitary fixation was approximately 5 min.

2.3. Histology

2.3.1. Fixation and sectioning

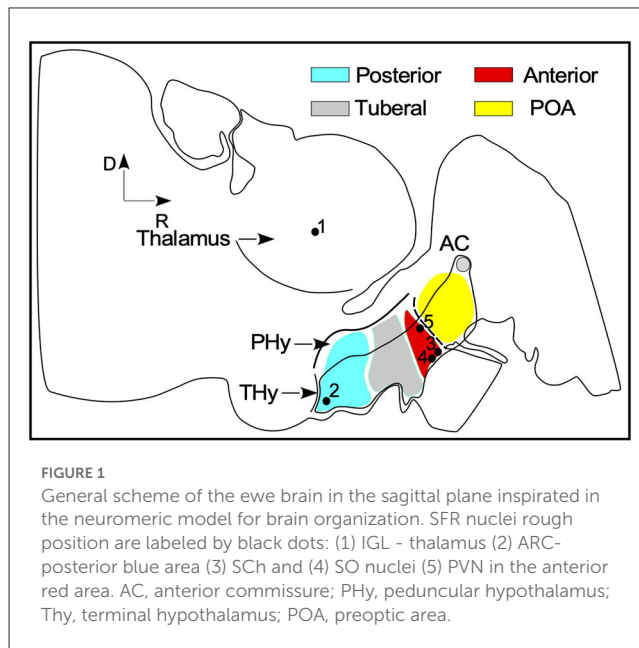
Each brain was placed in a biosafety container with 1500 ml of 4% paraformaldehyde in 0.1 M phosphate buffer, pH 7.4 at 4°C. After 48 h, to obtain standardized anatomical planes, the brains were coronally cut from the optic chiasm to 1 cm caudally to the mamillary body, yielding a squared block containing almost the entire diencephalon. Block tissues were fixed for one more week after renewing the fixation solution every 48 h and then immersed in solutions with increasing sucrose concentrations (from 20 to 100%) until they sank. Subsequently, diencephalic blocks were carved to obtain standardized cutting planes and sectioned serially in the coronal, sagittal or horizontal plane at 40 µm using a freezing microtome. For coronal sections, whole diencephalons (left and right sides: four animals) were used, whereas the rest of the diencephalons studied (two animals) were cut through the midline, using each side to prepare sagittal or horizontal sections. In addition, 3600 Nissl-stained coronal histological sections were obtained from the four diencephalons, whereas 900 sagittal and 900 horizontal Nissl-stained histological sections were obtained from the other two diencephalons. In total, 1080 coronal histological sections were used for calcium-binding proteins (CBPs) immunohistochemistry and 720 coronal histological sections for ionized calcium binding adaptor molecule 1 (IBA1) and glial fibrillary acid protein (GFAP) immunohistochemistry. After fixation, a 3% retraction occurred in the diencephalic blocks. After sectioning, in Nissl-stained sections, the thickness retraction was 4 microns, as calculated by three experienced microscopists using a x100 Leica plan apochromatic objective. Thus, histological sections stained with Nissl had an estimated final thickness of 36 µm.

2.3.2. Nissl staining

Sections were stained by immersion in 1% cresyl violet (C5042, Sigma-Aldrich, Merck KGaA, Darmstadt, Germany) for 10 min at pH 3.0 and in 96% alcohol + acetic acid for staining differentiation. Lastly, the sections were dehydrated in increasing alcohol concentrations, from 50 to 100%, followed by clearing in xylene (3 × 3 min), mounting and cover slipping. The nomenclature used in this paper followed that reported in the Paxinos' atlas of the mouse brain (41). SFR nuclei of this atlas were clearly recognized in our material. In addition, for an appropriate localization of SFR nuclei in the ewe brain, we followed the guidelines based on a recently updated neuromeric model developed in rodents (42) (Figure 1).

2.3.3. Immunostaining

Alternate coronal serial sections were stained for calbindin, calretinin, parvalbumin, IBA1 and GFAP (for details about the antibodies used, see Table 1). Free-floating sections were



sequentially washed with 0.05 M tris buffer saline, pH 7.6, followed by endogenous peroxidase inhibition by incubation in 10% methanol + 3% H₂O₂ in 0.1 M PB for 10 min. Subsequently, the sections were washed in 0.1 M PB and 0.05 M TBS-Tx, pH 8.0, 0.3% Triton X-100 (T9284 Sigma, St. Louis, MO, USA; TBS-Tx) and incubated with the corresponding primary antiserum (Table 1), for 48 h at 4°C. Non-specific labeling was blocked using fetal calf serum (10%). After washing three times in TBS-Tx, for 15 min, all sections were incubated with an anti-rabbit biotinylated secondary antibody (biotinylated anti-rabbit IgG H+L, BA-1000; Vector, Burlingame, CA, USA) or with an anti-mouse biotinylated secondary antibody (biotinylated anti rabbit IgG H+L, BA-2000; Vector, Burlingame, CA, USA) at a 1:200 dilution in TBS-Tx for 120 min at room temperature. The sections were then washed with TBS-Tx and incubated for 180 min in avidin/biotin-peroxidase (ABC complex, Vectastain Standard ABC kit PK-4000; Vector, Burlingame, CA, USA) and further washed with TBS-Tx, followed by Tris-HCl, pH 8.0. Lastly, the sections were incubated in 3,3-diaminobenzidine tetrahydrochloride (DAB; D-9015; Sigma-Aldrich, St. Louis, MO, USA) with 0.006% H₂O₂ to visualize the peroxidase reaction. Negative controls, processed without the corresponding primary antibody, were performed to confirm immunostaining specificity; in all cases, the results showed the specificity of the primary antibodies used in this research. Calcium-binding protein cell phenotype analysis across a high number of representative mammalian species showed that the types of positive neurons generally coincided among species. Previous analysis indicated that these proteins have a highly phylogenetically conserved molecular structure in the brain in general and in the cerebellum in particular (30, 43, 44). Thus, superior colliculus and cerebellum (Supplementary Figure 1) have been analyzed as positive controls, showing immunostaining properties similar to those reported for humans and other high mammals, such as the common marmoset (29). Antibodies used by us are not commercially validated for sheep. However, previous literature

TABLE 1 Characteristics of the antibodies and dilutions used in this study.

| Antigen | Dilution | Inmunogen | Description |
|-------------|--------------------------|---|--|
| Calbindin | SWANT CB38a 1:5000 | Recombinant rat calbindin D-28k (CB) | Polyclonal rabbit Swant Cat# CB38, RRID: AB_10000340 |
| Calretinin | SWANT SW/7697 1:2000 | Recombinant human calretinin containing a 6-his tag at the N-terminal | Polyclonal rabbit Swant Cat# CR 7697, RRID: AB_2619710 |
| Parvalbumin | Sigma P-3088 1:1000 | Frog muscle parvalbumin. | Monoclonal mouse Sigma-Aldrich Cat# P3088, RRID: AB_477329 |
| GFAP | Sigma G-6171 1:500 | Purified GFAP from pig spinal cord | Monoclonal mouse Sigma-Aldrich Cat # G6171, RRID: AB_1840893 |
| IBA1 | Wako 019-19741 1:1000 | C-terminus of Iba 1 (NPTGPPAKKAISELPC) | Polyclonal rabbit, Wako Cat # 019-19741, RRID: AB_839504 |

reported the use of these antibodies in sheep (45–48). In the case of the antibody against IBA1 used in our paper, we have performed a BLASTp analysis of the 16 amino acid epitope (NPTGPPAKKAISELPC) used as immunogenic protein against the sheep genome, and we have obtained 92.86% homology: Results for BLASTp against Sheep Oar_rambouillet_v1.0 [Proteins (Ensembl)] - Ovis_aries_rambouillet - Ensembl genome browser 108.

2.3.4. Image analysis

Panoramic mosaics of entire sections of the rostral half of the brain were captured at selected interaural coordinates. Digital photomicrographs (mosaics) were taken under a Leica DMRB microscope with X10 objectives (Leica Plan Apo), assembled using the “Virtual slice” module of NeuroLucida 8.0[®] (MBF-Bioscience, Williston, Vermont, USA), and adjusting the microscope illumination source before each image capture. To measure the area and perimeter of the cells, photomicrographs of Nissl-stained sections were processed in ImageJ 2.0 software. Using the automatic method of analysis by density threshold segmentation, a detection range was applied to select the appropriate outlines of cell bodies, which were visually inspected to avoid counting superimposed or confluent groups of cells. To enhance photographs by pseudo-color transformation, improving the delimitation of Nissl-stained panoramic neuronal nuclei, we used different Image J software plugins (ICA 3, Spectrum, and 16-color tables). To numerically assess differences in the density of coronal sections immunostained with IBA1, mean gray levels were analyzed (ImageJ program) in selected frames taken on the horizontal axis at different distances from the 3rd ventricle.

3. Results

3.1. Serial Nissl staining sections of the diencephalic and hypothalamic SFR nuclei

To set cytoarchitectonic boundaries in panoramic high-resolution images, nuclei were delimited by exploring differences in cell density, cellular shape and size, and Nissl staining intensity. In this study, the preoptic area (POA), the anterior and the posterior areas of the terminal hypothalamus (THy), were analyzed to more easily describe the localization of SFR (Figure 1). This

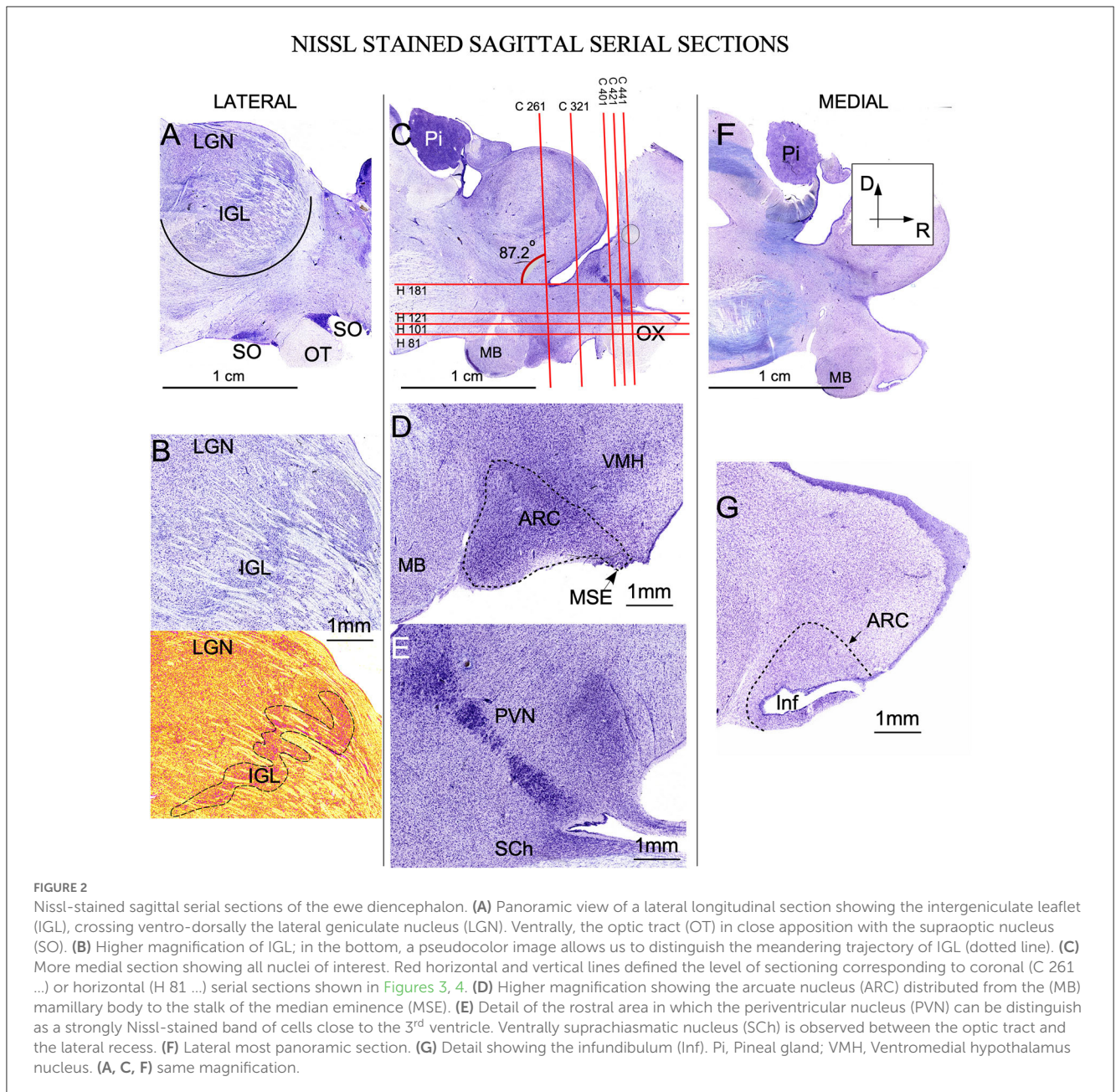
approach helped us to locate, in a single sagittal section, the four nuclei of interest, ARC in the posterior (Figure 1 dot 1), Sch and SO (Figure 1 dots 2, 3), in the anterior and PVN (Figure 1 dot 4) close to the POA. By contrast, in horizontal and coronal sections, the nuclei must be analyzed in several serial sections. To estimate the related position of coronal and horizontal sections with respect to the sagittal plane, the coordinates were calculated from the first rostral (for the coronal plane) and ventral (for the horizontal plane) sections from carved blocks of tissue (sectioning plane), by multiplying the order number in the series by the averaged thickness of the sections (36 μm) (Red lines in Figure 2C in correspondence with Figures 3, 4).

3.1.1. Intergeniculate leaflet of the thalamus

The thalamic lateral geniculate nucleus (LGN) was large (approximately 1 cm in the main diameter), oval, and located laterally and dorsally in the brain (Figure 2A). Pseudo-color images allowed us to define IGL borders easily and clearly in Nissl-stained sections after color conversion (Figure 2B bottom). Thus, in both sagittal (Figure 2A) and coronal planes (Figures 3A, G), IGL was identified by the snake plot shape of a high-density and hyperchromatic band of cells. This morphological feature facilitated the identification of the thalamic IGL in the border between the dorsal and ventral LGN. However, due to the presence of separate clusters and to its convoluted distribution, IGL was difficult to delimit in horizontal sections (not shown). IGL neuronal bodies were identified by their fusiform shape in the coronal plane and by their medium-to-large size (Area M: 649 μm^2 - SD \pm 346.6) (Figure 3G; Supplementary Table 1).

3.1.2. Arcuate nucleus

In sagittal sections, from its rostral limit with the mammillary body, ARC appeared as a ribbon of cells, distributed, along the entire ventricle extension to the infundibulum (Inf) and the median stalk eminence (Figures 2D, G, dotted line). In the ventral THy, in the coronal plane, ARC wrapped around the 3rd ventricle (Figures 3B, C) and was clearly distinguished for its strong Nissl staining, in all planes (Figures 2G, 4A–C). In horizontal sections, ARC was observed in the caudal third



of the 3rd ventricle (Figures 4A–C). In coronal sections, ARC was triangular, extended for approximately 3 mm dorsally, and showed strongly stained neurons (Figure 3H). Its neurons were medium to large (averaged area: 590 μm^2 – SD \pm 290.5), hyperchromatic, triangular and more densely packed in the ventral part (Supplementary Table 1).

3.1.3. Paraventricular nucleus

PVN was easily delimited, in all planes, because its neurons were large and strongly Nissl stained (Figures 2E, 3D, E, 4D). PVN had a columnar shape in the sagittal plane (Figure 1E) and a round shape in the coronal (Figures 2D, E) and horizontal (Figure 3D) planes. PVN neurons were spherical and large (averaged area: 899 μm^2 – SD \pm 322.4) (Figure 2I; Supplementary Table 1).

3.1.4. Suprachiasmatic nucleus

SCh was located medially and ventrally on the floor of the 3rd ventricle, bordering the optic tract and chiasma. SCh was small, round, or oval at the horizontal plane (Figure 4C), and conical at the sagittal (Figure 2E) and coronal (Figures 3E–I) planes. According to Nissl staining, SCh can be subdivided in ventral and dorsal areas. SCh neurons had different shapes of neuronal somata, mostly with stellate and oval contours, with small or medium sizes (Averaged area: 161.9 μm^2 – SD \pm 181.2) (Figure 3J; Supplementary Table 1).

3.1.5. Supraoptic nucleus

SO contained densely packed, large, and strongly Nissl-stained cell bodies. In the most rostral area, SO was elongated, slim,

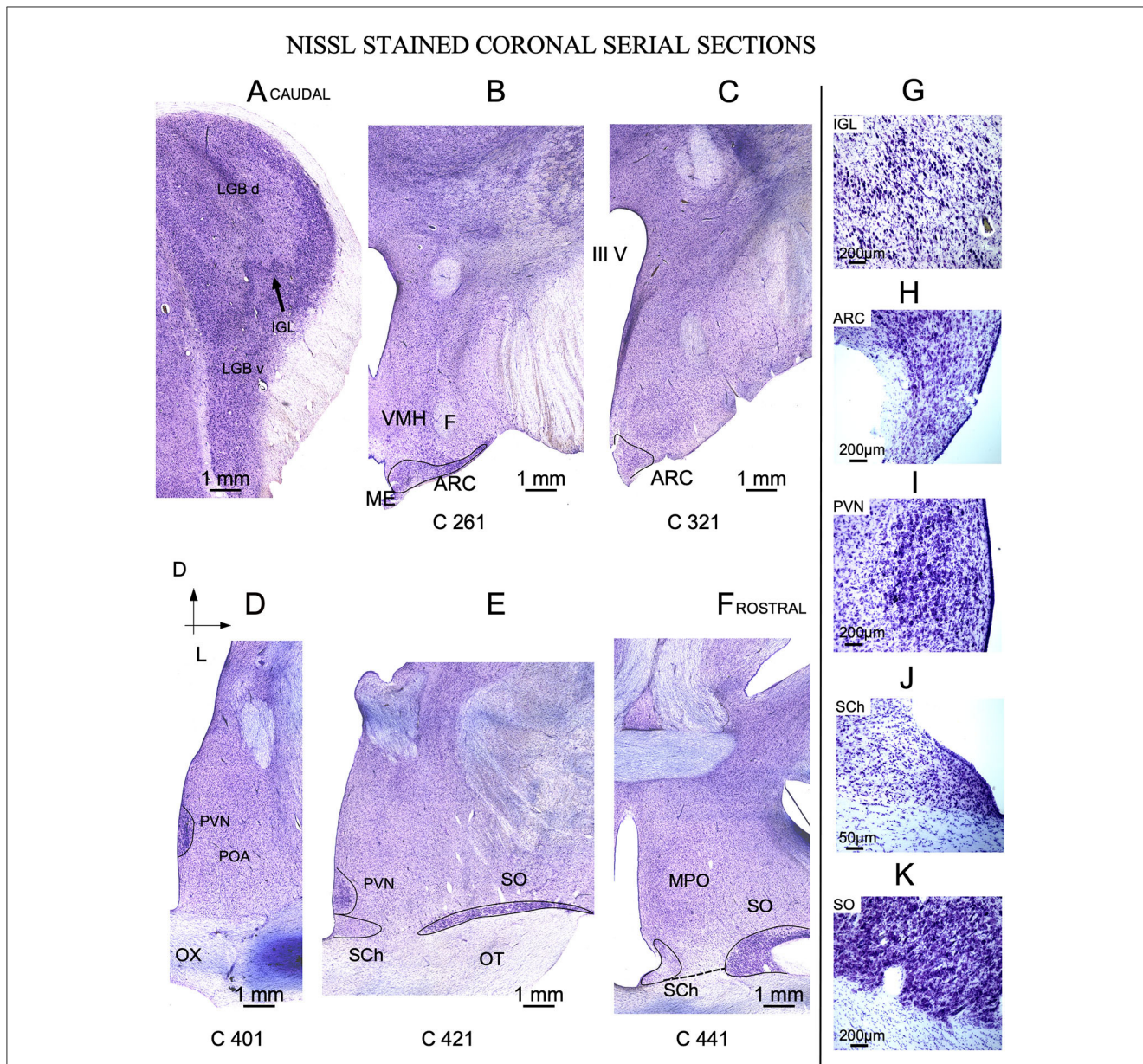
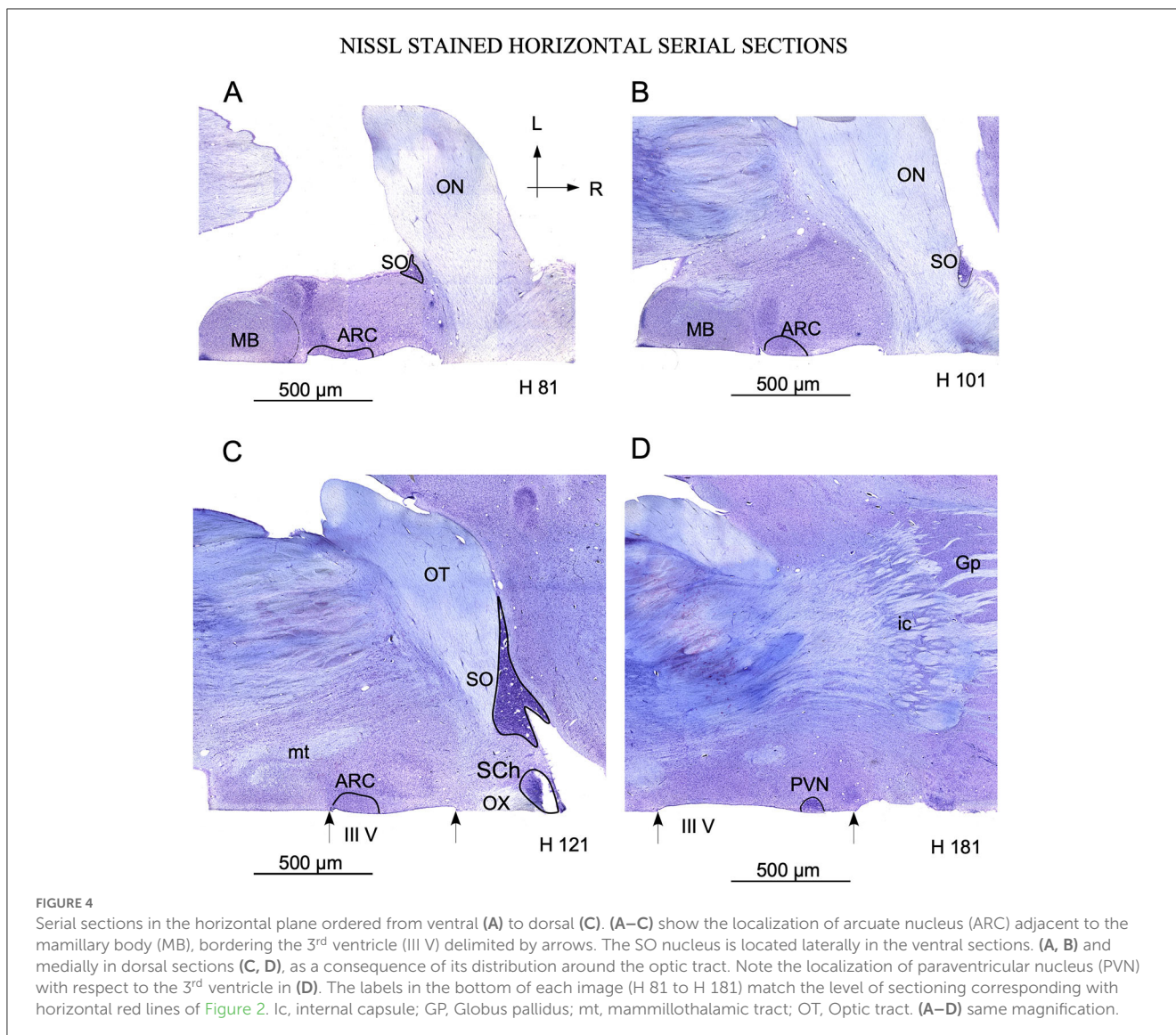


FIGURE 3
 Nissl-stained coronal serial sections. **(A)** Caudal section showing the dorsal (LGB d) and ventral (LGB v) divisions of the lateral geniculate body separated by the intergeniculate leaflet (IGL). **(B, C)** Arcuate nucleus (ARC) located in the caudal hypothalamic red area in Figure 1. **(D–F)** Three representative sections from the rostral hypothalamus (blue area in Figure 1). The labels in the bottom of each image (C 261 to C 441) match the level of sectioning corresponding with vertical red lines of Figure 2. **(G–K)** Details of Nissl-stained cells from all nuclei of interest. OX, Optic chiasm; MPO, Medial preoptic area; ME, Medial eminence; VMH, ventro-medial nucleus; III V, third ventricle- **(A–F)** same scale bar.

and oval in coronal sections (Figures 3E, F). Given its large size, this nucleus was observed along more than 20 rostral sections (Figures 3E, F). Because SO is close to the optic tract, at the most ventral horizontal plane, SO was identified at the lateral part of the most ventral horizontal sections (Figure 4A) and medially to the dorsal ones (Figure 4C). Thus, the optic tract and optic chiasm border the SO nucleus (Figures 2A, 3E, F, 4A–C), whose neurons are uniformly round or fusiform and large (Averaged area: $915 \mu\text{m}^2 - \text{SD} \pm 327.6$) (Figure 2K; Supplementary Table 1).

3.2. Neuronal morphological features and CBPs immunostaining of the diencephalic and hypothalamic SFR nuclei

The neurons of SFR nuclei showed Cb and Cr, but not Pv, immunoreactivity. All CBPs immunocytochemistry results from serial sections in the coronal plane were compared with the corresponding Nissl-stained alternate sections in the coronal plane.



3.2.1. Intergeniculate leaflet of the thalamus

Cb and Cr -stained sections showed, in IGL, restricted immunopositively terminal buttons, which made it possible to delineate the nucleus from LG subdivisions (Figures 5A–D). By immunoreactivity against Cr, dense oval cell bodies were observed (Figures 5C, D), as in Nissl-stained sections (Figure 3G). In Pv immunostained sections, the intense positive reaction along LGN blurred the nucleus, making it difficult to determine a specific reactivity in cell bodies (not shown).

3.2.2. Arcuate nucleus

In ARC, stellates cells were immunoreactivity against Cb and Cr (Figures 5E–G). Those showing immunoreactivity to Cb were a specific group of stellate multipolar medium or small neurons with a large number of dendrites (Figures 5E, F). Cr-immunoreactive neurons were dispersed in the most ventral part, near the third

ventricle (Figure 5G), such as small neurons observed in Nissl-stained sections (Figure 3H).

3.2.3. Paraventricular nucleus

PVN neurons were not immunoreactive to Pv and Cr (data not shown) but were immunoreactive to Cb, which allowed us to observe large multipolar neurons with well-defined cell bodies and well-defined dendrites (Figures 5H–K). Similarly, in Nissl-stained sections neurons from PVN were large and round (Figure 3I).

3.2.4. Suprachiasmatic nucleus

SCh contained Cb-immunoreactive neurons and showed positive fibers from the optic chiasm entering the nucleus, generating a dense terminal field (Figures 5L, M). After comparing immunoreactive against Cb with equivalent Nissl-stained sections, only a few of the Nissl-stained neurons (Figure 3J) were positive for this antibody (Figure 5L).

CALCIUM BINDING IMMUNOCYTOCHEMISTRY IN CORONAL SECTIONS

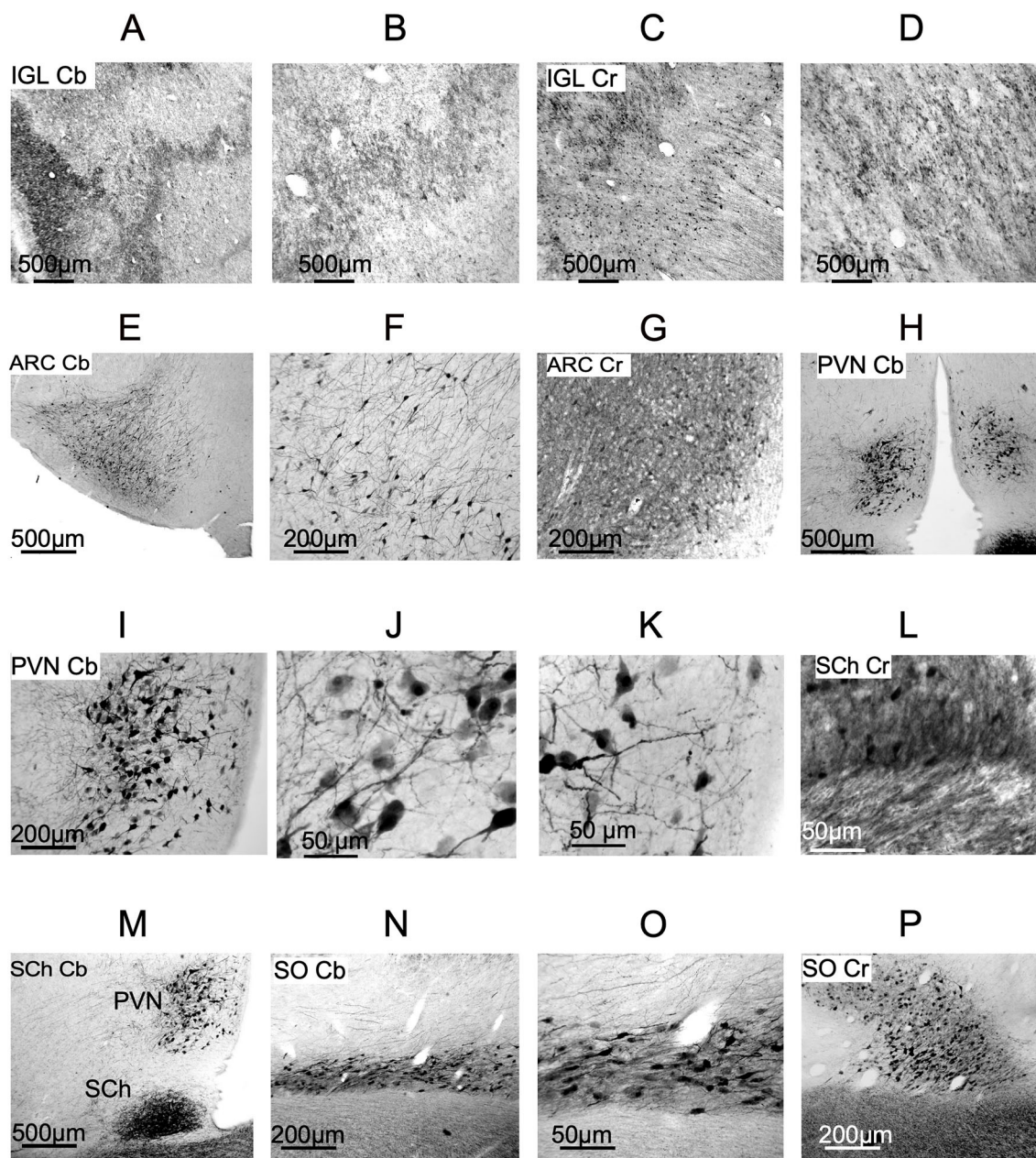


FIGURE 5

Calcium-binding protein immunoreactivity of the nuclei of interest (SFR). (A–D) Immunostaining of the IGL. Terminals are positive for calbindin and calretinin (E–G) Immunostaining of arcuate nucleus. Cb and Cr-stained neurons are evident. (H–K) Immunostaining of PVN. Large stellate neurons with thick dendrites are Cb positive. (L, M) Immunostaining of SCh. Cr and Cb positive fibers enter the nucleus from the optic chiasm [this photograph is a wider view of (H)]. (N–P) Immunostaining of SO, showing large Cb and Cr neurons oriented in the main axis of the nucleus.

3.2.5. Supraoptic nucleus

In our material, most SO neurons were immunopositive again Cb and/or Cr (Figures 5N–P). Immunopositively stained dendrites and cell bodies showed strong Cb and Cr staining (Figures 5N–P). Its medium-to-large neurons shows strongly immunopositive dendrites. Immunostained sections showed much smaller number of cells than the Nissl-stained ones (compare Figures 5N–P with Figure 2K).

3.3. Glial architecture IBA 1 and GFAP immunohistochemistry

No distinct features of astroglia and microglial cells were detected in IGL with respect to the remaining lateral geniculate body (not shown). In panoramic views, glial cell size and cell density were increased in extensive areas around ventricles in POA (rostral to the hypothalamus) and PHy, both for IBA 1 and

IBA 1 IMUNOCYTOCHEMISTRY CORONAL SERIAL SECTIONS

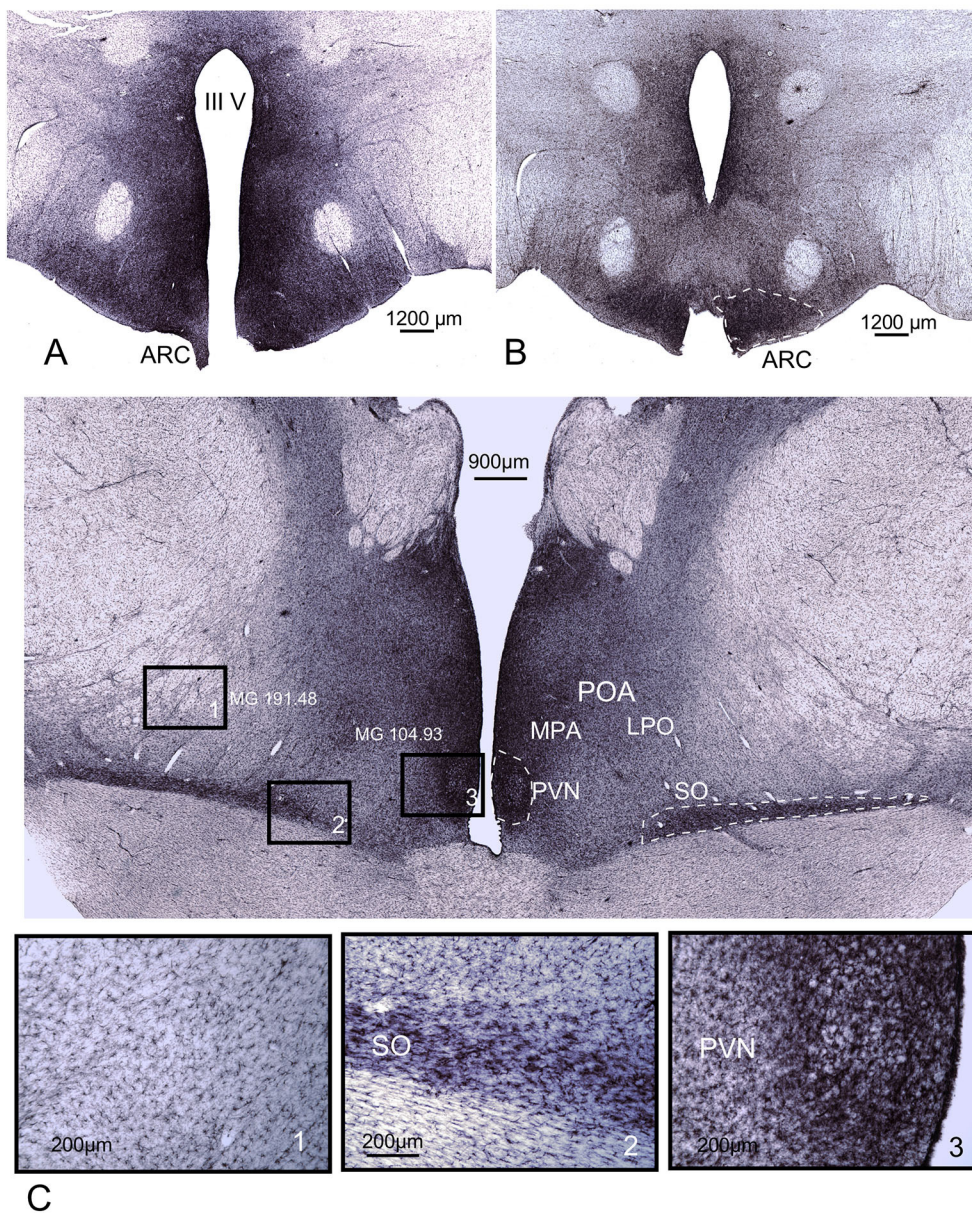


FIGURE 6
 IBA1 immunoreactivity in serial coronal sections. **(A, B)** caudal ventromedial hypothalamus. Densest microglial reaction is found in the ARC (dotted line) and around the 3rd ventricle. **(C)** POA. Details in squares from 1 to 3 (bottom of the figure) show that reactive microglial cells are highly dense and more concentrated around and inside PVN and SO nuclei. Note the intense staining around the 3rd ventricle in all levels of sectioning. Mean gray level measured inside the squares (MG – mean gray value).

GFAP immunocytochemistry (Figures 6, 7). In our material, medial (MPA) and lateral (LPO) regions of POA were distinguished based on differences in staining. IBA 1 immunoreaction labeled both areas, but GFAP immunoreaction only labeled MPA (compare Figures 6, 7).

Inside the POA and PHy, an intense immunoreaction in microglial and astroglial cells was observed inside SFR nuclei (Figures 5, 6 dotted lines). In PHy, a high concentration of IBA1-immunoreactive cells was identified along the border of the 3rd ventricle to the ventral area around and inside ARC

(Figures 6A, B dotted line); however, the density of immunoreactive cells decreased in the infundibular area, allowing us to define an ARC microglial-specific region separate from the periventricular zone (Figures 6A, B).

In IBA1 immunostained sections, from PVN and the 3rd ventricle, to the lateral limit of LPO, cell density decreased gradually dorsally and laterally, as shown after comparing gray density values from selected square areas in Figure 5C (mean gray values: Square 1 – 191.48/ Square 3 – 104.9). MPA and LPO limits were also well defined by the laterally

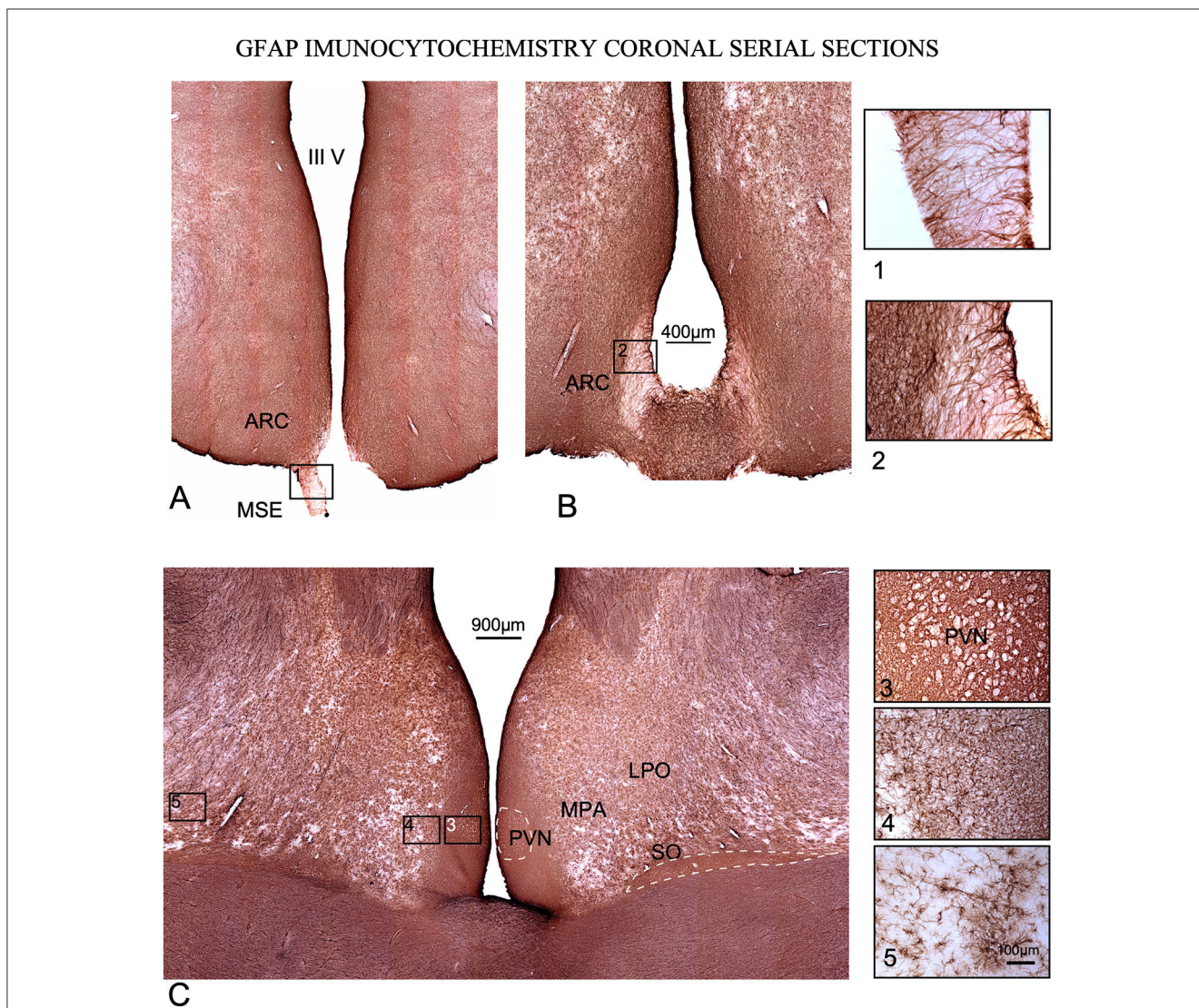


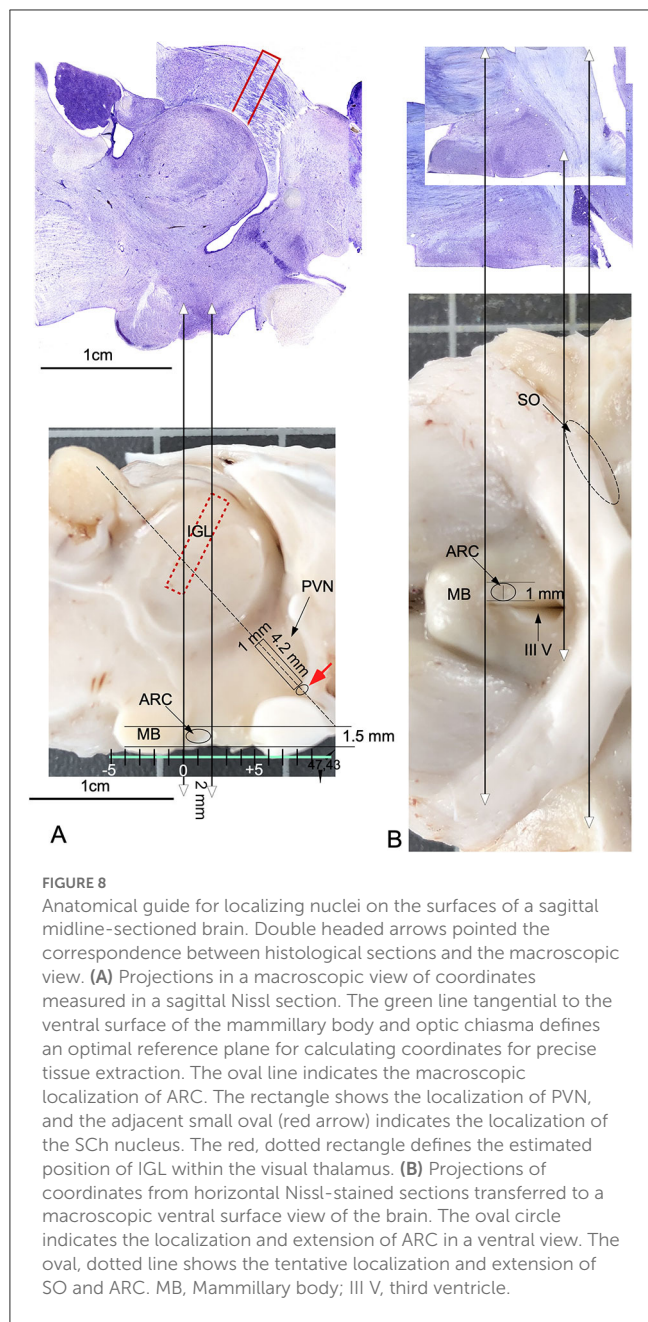
FIGURE 7
 GFAP immunoreactivity in coronal serial sections. **(A, B)** caudal sections. Squares (1) and (2), tanycytes at the median stalk eminence (MSE). **(C)** Rostral section. Higher cell density is observed around the 3rd ventricle in all levels of sectioning, and around and inside PVN and SO nuclei (dotted lines). Squares 3, 4, and 5 are shown at a higher magnification on the right of the figure. (3) Detail of immunoreactivity in PVN. Neurons encircled by astrocytes are shown as white contours. (4) Interstitial astroglia in the lateral preoptic area (LPO). (5) Non-reactive astrocytes far from the 3rd ventricle.

and dorsally slight decrease in immunoreactive microglial cells (Figure 6).

GFAP immunoreactivity also showed a high concentration of astrocytes around the ventricle and POA, but the densest reactive areas were more restricted to the paraventricular zone (Figure 6C). As in IBA1 sections, GFAP immunostaining density decreased laterally in POA, matching MPA and LPA borders (e.g., please note these differences in cell density in details 2, 3 and 4 in Figure 7). In GFAP-immunostained sections, PVN neurons appeared as negative dots framed by densely stained astrocytic feeds (Figure 7C square 3). In the most caudal, sections immunostained against GFP show tanycytes which cross the stalk and the median eminence forming a superficial well-stained limit and a superficial barrier (Figures 7A, B squares 1 and 2).

3.4. Macroscopic localization of nuclei in Nissl-stained sections

Measurements of the main central axis of the mammillary body in the three sectioning planes in histological Nissl-stained sections, compared with measures in macroscopic images, show small differences in retraction (<3%). As mentioned above, with measurements of the thickness of 20 randomly selected sections taken by three different observers (z-axis, and using a Leica X100 plan apo objective), we calculated a shrinkage of 4 (+/-) µm (final averaged thickness 36 µm). These data facilitated slight corrections in the translation of coordinates using the fixation and sectioning protocol applied here. Moreover, when coordinates are translated from frozen specimens, which is the most suitable approach to tissue extraction for molecular analysis, the measurements must



be modified after evaluating changes in tissue contraction in each procedure. For micro-dissection, coordinates for extraction were defined in present paper in a caudal-to-rostral direction taking as referent point the anterior limit of the mammillary body (easily located macroscopically by its spherical shape close to the midline). From this reference point, ARC was localized in a sagittal view at 1.5 mm at the vertical axis, 2 mm at the horizontal axis (Figure 8A), and 1 mm laterally to midline (Figure 8B). By using as a reference, a parallel line to the ventral surface (tangential to the ventral most point of the mammillary body and the surface of the optic tracts – green line in Figure 8A), the periventricular region was located at its main axis oriented in an angle of 47.43°. By using the same reference line, SCh specimens were localized 0.7 mm dorsally to the recess (Figure 8A, red arrows), and PVN was dissected by

cutting a 4.2 × 1 mm rectangle (Figure 8A rectangle). Due to its localization, sandwiched between the optic tract (OT) and the preoptic area, SO coordinates cannot be accurately defined, but a tentative localization is suggested in Figure 8B (black dotted line). Furthermore, by its convoluted structure and oblique orientation, IGL coordinates are very difficult to precisely define in macroscopic views; nevertheless, a tentative localization is also provided in Figure 8 (red dotted rectangle).

4. Discussion

4.1. General considerations

After SFR nuclei activation by changes in photoperiod, peptide regulation induces neuronal activation and plasticity (11–13) leading to morphological changes in the hypothalamus. These changes in the estrous cycle, previously studied in rats (49) and as a function of seasonal fluctuations, mainly regulated by melatonin (33) may induce size and shape differences in SFR nuclei. In this study, ewes were euthanized under specific environmental, nutritional, and estrous cycle conditions. However, potential changes in morphology may be induced by plastic reorganization after changes in hormonal induction. Therefore, the anatomical data reported here must be revised under other estral conditions.

Relative SCh, ARC and PVN differences in shape and localization were identified in this study. SO showed substantial qualitative differences in both its layout and relative size in ewes, compared with other mammals (e.g., rodents, primates, pigs) (26, 31); however, the basic neuroanatomical plan of organization of ewe SFR nuclei, is similar to that of other mammals.

In line with differences in reproductive functions between rams (e.g., mounting) and Ewes (e.g., pregnancy and lactation), strong anatomical differences have been previously shown in the nuclei studied here (sexual dimorphism) (50, 51). Accordingly, in the future a specific anatomical systematization should be performed in rams for a complete neuroanatomical description of nuclei involved in seasonality in sheep (*Ovis orientalis aries*).

KNDy neurons form an interconnected network that fires synchronously to drive GnRH release during a pulse, inducing combined differences between nuclei closely positioned in the hypothalamus (23, 24). For future molecular analysis, functional and anatomical interconnections between hypothalamic nuclei involved in seasonal sexual activation should be studied using well-defined samples of tissue restricted to specific nuclei. A study using nuclei microdissection to analyze large areas of the hypothalamus quickly immersed in liquid nitrogen reported excellent results about changes in GnRH-R mRNA levels after stress in merino sheep (52). Thus, in the present study, we provide a cytoarchitectonic guide for a more precise microdissection of SFR nuclei, enabling researchers to collect more appropriate samples for conventional proteomic or genomic techniques, individual cell sequencing or chemical analysis of hormones, transcription factors, and peptides. Preparing serial sagittal sections after micro-dissection enables to confirm the appropriate extracted areas, as previously we reported in the rat (53).

4.2. Intergeniculate leaflet nucleus

IGL was first described in rats (54), and golden hamsters (55) as a well-defined band of cells located between the dorsal and ventral medial geniculate bodies. When comparing rodents and higher mammals, such as primates (26) or sheep (present results), the well-defined straight band between dorsal and ventral subdivisions of the visual thalamus were masked and hidden by the complex laminar organization of the dorsal geniculate bodies. However, in our Nissl-stained sheep sections (Figure 2A), large fusiform neurons, delimiting IGL, were more clearly observed in the coronal plane (Figure 3G). In rodents, nevertheless, its architecture is well defined, but both the localization and limits are difficult to distinguish in some gyrencephalic vertebrate species (26) because primates once had a generic wide pregeniculate nucleus (PGN) included both the ventral geniculate nucleus and IGL (56). In the visual thalamus of the rock cavy (*Kerodon rupestris*; rodent), IGL is identified as a well-defined and straight band between dorsal and ventral subdivisions, but in marmosets (primates), this subdivision is masked and hidden by the complex laminar organization of the dorsal part of the LG (57). Due to its intricate architectonic organization, the primate IGL should be neuroanatomically better defined by using additional neurochemical markers (e.g., VIP immunocytochemistry). However, in the ewe, positive Cb and Cr terminal fields, most likely coming from the retina, allowed us to trace the borders of this subdivision. In summary, due to its larger fusiform neurons and Cb and Cr immunoreactivity (Figures 5B, C), IGL can be well differentiated from the remaining visual thalamus in the ewe (Figure 3A).

4.3. Arcuate nucleus

Anatomically, six types of neurons have been described in previous studies using the Golgi method in the rat ARC nucleus (58). Different neurochemical phenotypes have also been reported, particularly a neuronal type in which kisspeptin, neurokinin A and dynorphin coexist, known as KNDy neurons (59). These key neurons regulate seasonality outputs for reproduction (kisspeptin, neurokinin, dynorphin) by activating GnRH pulses in sheep (32). Because these neurons are mainly located in ARC (23, 60), techniques demonstrating kisspeptin, neurokinin or dynorphin (not available in our material) should be used as complementary markers to be able to better correlate the morphology and topography of this nuclei with present results. In ARC, several chemical neuronal types have also been described; thus, an accurate analysis in the ewe will require a peptide immunocytochemistry analysis, which was not performed in our study. Nevertheless, in our material, the morphology (Nissl) and immunoreactivity (CBPs) of dorsal ARC neurons showed that they were roughly similar in size and location to KNDy neurons.

4.4. Paraventricular nucleus

PVN shows the highest peptidergic and glial activity in the hypothalamus and is located at the border of the third ventricle.

Surrounding this structure, some regions of special interest for their association with seasonal reproduction in sheep, such as the set of A15 dopaminergic cells, regulate the negative feedback of estradiol, which in turn is another compound that regulates both GnRH production and pulses (32, 61, 62). In ewes, the columnar distribution at the sagittal plane allowed us to distinguish strongly Nissl-stained neurons into three potential subdivisions (Figure 2E).

4.5. Suprachiasmatic nucleus

Light cycle-sensitive pacemaker SCh neurons are directly regulated by retinal and indirectly by IGL projections through the geniculate thalamic tract (63). SCh, a highly phylogenetically conserved structure with a similar location in many species of vertebrates, is placed between the 3rd ventricle and the optic chiasm and contains small and packed neurons (64). In ewes, we also observed small neurons (~430 μm^2) and strong immunoreactivity for fibers containing Cr or Cb presumably belonging to retinal projections (Figures 5L, M).

4.6. Supraoptic nucleus

SO interconnects several of the seasonality nuclei (PVN and ARC), directly projecting to the pituitary gland and to the region surrounding the third ventricle (44, 45). Because SO is involved in glial activation, we will analyze its morphological features more extensively in the next section (51). Despite differences in animal size, SO nucleus and its neurons are much larger in ewes than in rodents, but they have the same topographical distribution (26, 41).

4.7. Glial architecture

To our best knowledge, this is the first analysis of glial cell architecture in the ewe hypothalamus and diencephalon. Glial cells are widely known to play a key role in the synthesis, recycling and delivery of hypothalamic hormones and factors (65) and thus GnRH in the hypothalamus of different mammals, including sheep (51, 66, 67). Increases in cell density and cell size around the 3rd ventricle shown in our material after IBA1 and GFAP immunoreactivity, indeed expresses glial overactivation (increase cell size, number of profiles, immunostaining and cell density) which can be related to potential areas of higher metabolic regulation of sexual hormones (GnRH) (68). Accordingly, the densest areas of microglial and astroglia immunoreaction around PVN and SO, in the anterior hypothalamus, and around the ARC, in the THy, may be related with a heightened endocrine or paracrine regulation.

Notwithstanding the above, both types of reactive glial cells (as shown by larger and denser population of microglia and astrocytes) are found around neurons. These findings suggest the potential role of denser immunoreactive areas with overactivated paracrine secretion. When comparing IBA1 and

GFAP immunoreactivity, microglial reactivity was more extended in all section levels, suggesting a microglial more widespread in areas potentially implicated in secretory regulation (please compare Figures 6, 7). Tanycytes formed a dense ventricular barrier of the 3rd ventricle in the stalk-median eminence (Figures 7A, B squares 1, 2). Due to the absence of any other reactive glial cells, this finding suggests that these areas, as in other species, regulate the access of metabolic signals to the hypothalamus (69).

4.8. Concluding remarks

Our results establish a guide for future histological, physiological and molecular experiments related to hypothalamic effects of interventions in farm animals aimed at improving fertility regulation (e.g., GnRH neurons, KNDy cells, and melatonin receptors). The data provided here may also have translational relevance because the sheep brain, considering its similarity in anatomy and organization, is a good experimental model for human neuroanatomical research, as recently suggested (70). Finally, by establishing a procedure for the section-to-brain translation of coordinates, this research may also help us to develop suitable procedures for nuclei/tissue extraction from specific nuclei of interest toward assessing changes in mRNA levels by RT-PCR or in protein levels by Western blot.

Data availability statement

The raw data supporting the conclusions of this article will be made available by the authors, without undue reservation.

Ethics statement

The animal study was reviewed and approved by the University of Salamanca.

Author contributions

MM and CP designed the experiments. MM and IP perform the experiments. MM and RC wrote the paper. CP and JA participated in the discussion of the results and corrected the manuscript. All authors contributed to the article and approved the submitted version.

References

- Chemineau P, Guillaume D, Migaud M, Thiéry JC, Pellicer-Rubio MT, Malpoux B. Seasonality of reproduction in mammals: intimate regulatory mechanisms and practical implications. *Reprod Domest Animals*. (2008) 43:40–7. doi: 10.1111/j.1439-0531.2008.01141.x
- Espinoza-Flores LA, Andrade-Esparza JD, Hernández H, Zarazaga LA, Abecia JA, Chemineau P, et al. Male effect using photostimulated bucks and

Funding

This study was supported by the Spanish Ministry of Science and Innovation (Ministerio de Ciencia e Innovación – MICINN) Grant number: PID2020-117266RB-C21.

Acknowledgments

The authors would like to thank Dr. Paloma Merchan for her useful suggestions about neuroanatomical nomenclature and Dr. Herrero Turrion for his invaluable advices about antibodies characterization. The authors also would like to thank MACRISA Slaughterhouse for providing ewes tissue, and Carlos V. Melo for proofreading this manuscript.

Conflict of interest

The authors declare that the research was conducted in the absence of any commercial or financial relationships that could be construed as a potential conflict of interest.

Publisher's note

All claims expressed in this article are solely those of the authors and do not necessarily represent those of their affiliated organizations, or those of the publisher, the editors and the reviewers. Any product that may be evaluated in this article, or claim that may be made by its manufacturer, is not guaranteed or endorsed by the publisher.

Supplementary material

The Supplementary Material for this article can be found online at: <https://www.frontiersin.org/articles/10.3389/fvets.2023.1101024/full#supplementary-material>

SUPPLEMENTARY FIGURE 1

Positive controls for immunocytochemistry. (A) Superior colliculus (SC) immunostained against calretinin. (B) SC immunostained against Calbindin and (C) SC immunostained against parvalbumin. The Intermediate white layer (InWH) show immunopositive fibers for calretinin and parvalbumin but not for calbindin. Zo. zona layer, SuG superficial gray layer, Op optic nerve layer, InWH intermediate white layer, DpG Deep gray layer. (D) Parvalbumin immunostained of the ewe cerebellum. Note the intense immunoreactivity of basket cells and its pericellular nests, as well as positive fibers in white matter sera. ML, molecular layer, PCL, Purkinje layer, GCL, granule cell layer, WM, white matter.

SUPPLEMENTARY TABLE 1

Data summary table.

- nutritional supplementation advance puberty in goats under semi-extensive management. *Theriogenology*. (2020) 143:82–7. doi: 10.1016/j.theriogenology.2019.12.005

- Abecia JA, Forcada F, González-Bulnes A. Hormonal control of reproduction in small ruminants. *Anim Reprod Sci*. (2012) 130:173–9. doi: 10.1016/j.anireprosci.2012.01.011

4. Varpe O. Life history adaptations to seasonality. *Integrative and Comparative Biology*. Oxford: Oxford University Press (2017). p. 943–960.
5. Chowdhury S, Zalucki MP, Amano T, Woodworth BK, Venegas-Li R, Fuller RA. Seasonal spatial dynamics of butterfly migration. *Ecol Lett.* (2021) 24:1814–23. doi: 10.1111/ele.13787
6. Heldstab SA, van Schaik CP, Müller DWH, Rensch E, Lackey LB, Zerbe P, et al. Reproductive seasonality in primates: patterns, concepts and unsolved questions. *Biological Reviews.* (2021) 96:66–88. doi: 10.1111/brv.12646
7. Rojansky N, Brzezinski A, Schenker JG. Seasonally in human reproduction: an update. *Human Reprod.* (1992) 7:735–45. doi: 10.1093/oxfordjournals.humrep.a137729
8. Clarke IJ, Smith JT, Caraty A, Goodman RL, Lehman MN. Kisspeptin and seasonality in sheep. *Peptides.* (2009) 30:154–63. doi: 10.1016/j.peptides.2008.08.022
9. Tsartsianidou V, Kapsona VV, Sánchez-Molano E, Basdagianni Z, Carabaño MJ, Chatziplis D, Arsenos G, Triantafyllidis A, Banos G. Understanding the seasonality of performance resilience to climate volatility in Mediterranean dairy sheep. *Sci Rep.* (2021) 11:8. doi: 10.1038/s41598-021-81461-8
10. Balaro MFA, de Mello SGV, da Silva Santos A, Cavalcanti LM, Almosny NRP, Fonseca JF, et al. Reproductive seasonality in Saanen goats kept under tropical conditions. *Tropical Anim Health Prod.* (2019) 51:345–53. doi: 10.1007/s11250-018-1696-2
11. Migaud M, Buttrill L, Batailler M. Seasonal regulation of structural plasticity and neurogenesis in the adult mammalian brain: focus on the sheep hypothalamus. *Front Neuroendocrinol.* (2015) 37:146–57. doi: 10.1016/j.yfrne.2014.11.004
12. Hazlerigg DG, Wyse CA, Dardente H, Hanon EA, Lincoln GA. Photoperiodic variation in CD45-positive cells and cell proliferation in the mediobasal hypothalamus of the soay sheep. *Chronobiol Int.* (2013) 30:548–58. doi: 10.3109/07420528.2012.754450
13. Batailler M, Derouet L, Buttrill L, Migaud M. Sensitivity to the photoperiod and potential migratory features of neuroblasts in the adult sheep hypothalamus. *Brain Struct Funct.* (2016) 221:3301–14. doi: 10.1007/s00429-015-1101-0
14. Hong L, Jiang Q, Long S, Wang H, Zhang L, Tian Y, et al. Valproic acid influences mtnr1a intracellular trafficking and signaling in a β -arrestin 2-dependent manner. *Mol Neurobiol.* (2016) 53:1237–46. doi: 10.1007/s12035-014-9085-y
15. Messer LA, Wang L, Tuggle CK, Yerle M, Chardon P, Pomp D, et al. Mapping of the melatonin receptor 1a (MTNR1A) gene in pigs, sheep, and cattle. *Mammalian Genome.* (1997) 9:368–70. doi: 10.1007/s00335990044
16. He X, Zhang Z, Chu M. The effect of SNP rs400827589 in exon 2 of the MTNR1B gene on reproductive seasonality and litter size in sheep. *Vet Med Sci.* (2020) 6:804–12. doi: 10.1002/vms3.280
17. Abecia JA, Mura MC, Carvajal-Serna M, Pulinas L, Macías A, Casao A, et al. Polymorphisms of the melatonin receptor 1A (MTNR1A) gene influence the age at first mating in autumn-born ram-lambs and sexual activity of adult rams in spring. *Theriogenology.* (2020) 157:42–7. doi: 10.1016/j.theriogenology.2020.07.030
18. Dardente H. Melatonin-dependent timing of seasonal reproduction by the pars tuberalis: pivotal roles for long day lengths and thyroid hormones. *J Neuroendocrinology.* (2012) 24:249–66. doi: 10.1111/j.1365-2826.2011.02250.x
19. Hileman SM, McManus CJ, Goodman RL, Jansen HT. Neurons of the lateral preoptic area/rostral anterior hypothalamic area are required for photoperiodic inhibition of estrous cyclicity in sheep. *Biol Reprod.* (2011) 85:1057–65. doi: 10.1095/biolreprod.111.092031
20. Abecia JA, Keller M, Chemineau P, Delgado JA. Light-induced sexually active rams provoke LH preovulatory surges and enhances LH concentrations in ewes after progestagen treatment. *Heliyon.* (2020) 6:e03529. doi: 10.1016/j.heliyon.2020.e03529
21. Abecia JA, Keller M, Palacios C, Chemineau P, Delgado JA. Light-induced sexually active rams prevent the seasonal inhibition of luteinizing-hormone in ovariectomized estradiol-implanted ewes. *Theriogenology.* (2019) 136:43–6. doi: 10.1016/j.theriogenology.2019.06.032
22. Carvajal-Serna M, Fatnassi M, Torres-Ruda F, Cardozo JA, Grajales-Lombana H, Hammadi M, et al. Vasectomy and photoperiodic regimen modify the protein profile, hormonal content and antioxidant enzymes activity of ram seminal plasma. *Int J Mol Sci.* (2020) 21:1–13. doi: 10.3390/ijms21218063
23. Merkle CM, Coolen LM, Goodman RL, Lehman MN. Evidence for changes in numbers of synaptic inputs onto Kndy and GnRH neurons during the preovulatory LH surge in the ewe. *J Neuroendocrinol.* (2015) 27:624–35. doi: 10.1111/jne.12293
24. Lehman MN, Coolen LM, Goodman RL. Importance of neuroanatomical data from domestic animals to the development and testing of the KNDY hypothesis for GnRH pulse generation. *Domestic Anim Endocrinol.* (2020) 73:106441. doi: 10.1016/j.domaniend.2020.106441
25. Robinson JE, Birch RA, Grindrod JA, Taylor JA, Unsworth WP. Sexually differentiated regulation of GnRH release by gonadal steroid hormones in sheep. *Reprod Suppl.* (2003) 61:299–310. doi: 10.1530/biosciproc.5.022
26. Cavalcante JS, Britto LRG, Toledo CAB, Nascimento ES, Lima RRM, Pontes ALB, et al. Calcium-binding proteins in the circadian centers of the common marmoset (*Callithrix jacchus*) and the rock cavy (*Kerodon rupestris*) brains. *Brain Res Bull.* (2008) 76:354–60. doi: 10.1016/j.brainresbull.2008.02.028
27. Merkle CM, Shuping SL, Nestor CC. Neuronal networks that regulate gonadotropin-releasing hormone/luteinizing hormone secretion during undernutrition: evidence from sheep. *Domestic Anim Endocrinol.* (2020) 73:106469. doi: 10.1016/j.domaniend.2020.106469
28. Weems PW, Coolen LM, Hileman SM, Hardy S, McCosh RB, Goodman RL, et al. Evidence that dynorphin acts upon KNDY and GnRH neurons during GnRH pulse termination in the ewe. *Endocrinology.* (2018) 159:3187–99. doi: 10.1210/en.2018-00435
29. Chong MHY, Worthy KH, Rosa MGP, Atapour N. Neuronal density and expression of calcium-binding proteins across the layers of the superior colliculus in the common marmoset (*Callithrix jacchus*). *J Comp Neurol.* (2022) 530:2966–76. doi: 10.1002/cne.25388
30. Hof PR, Glezer II, Condé F, Flagg RA, Rubin MB, Nimchinsky EA, et al. Cellular distribution of the calcium-binding proteins parvalbumin, calbindin, and calretinin in the neocortex of mammals: phylogenetic and developmental patterns. *J Chem Neuroanat.* (1999) 16:77–116. doi: 10.1016/S0891-0618(98)00065-9
31. Ettrup KS, Sørensen JC, Bjarkam CR. The anatomy of the Göttingen minipig hypothalamus. *J Chem Neuroanat.* (2010) 39:151–65. doi: 10.1016/j.jchemneu.2009.12.004
32. Nestor CC, Bedenbaugh MN, Hileman SM, Coolen LM, Lehman MN, Goodman RL. Regulation of GnRH pulsatility in ewes. *Reproduction.* (2018) 156:R83–99. doi: 10.1530/REP-18-0127
33. Revel FG, Masson-Pévet M, Pévet P, Mikkelsen JD, Simonneau V. Melatonin controls seasonal breeding by a network of hypothalamic targets. *Neuroendocrinology.* (2009) 90:1–14. doi: 10.1159/000219588
34. Vanderwolf CH, Cooley RK. *The Sheep Brain - A Photographic Series*. London: A J Kirby Co. (2002).
35. Ella A, Delgado JA, Chemineau P, Keller M. Computation of a high-resolution MRI 3D stereotaxic atlas of the sheep brain. *J Comp Neurol.* (2017) 525:676–92. doi: 10.1002/cne.24079
36. Sunagawa K, Nagamine I, Fujino T, Nakatsu Y, Hikosaka K. Stereotaxic atlas of the goat brain for an accurate approach to the hypothalamic nuclei. *Physiol Behav.* (2015) 145:91–105. doi: 10.1016/j.physbeh.2015.03.030
37. Coveñas R, Mangas A, Medina LE, Sánchez ML, Aguilar LA, Díaz-Cabiale Z, et al. Mapping of somatostatin-28 (1-12) in the alpaca diencephalon. *J Chem Neuroanat.* (2011) 42:89–98. doi: 10.1016/j.jchemneu.2011.06.006
38. Rogers JM. *A stereotaxic atlas of the diencephalon of the Southdown Sheep. Doctoral Dissertation - North Texas State University*. Denton, TX, United States. (1976)
39. Motomura K, Kosaka T. Medioventral part of the posterior thalamus in the mouse. *J Chem Neuroanat.* (2011) 42:192–209. doi: 10.1016/j.jchemneu.2011.07.004
40. Dávila JC, Guirado S, Puelles L. Expression of calcium-binding proteins in the diencephalon of the lizard *Psammodromus algerus*. *J Comp Neurol.* (2000) 427:67–92. doi: 10.1002/1096-9861(20001106)427:1<67::AID-CNE5>3.0.CO;2-2
41. Paxinos G, Franklin KBJ, Franklin KBJ. *The Mouse Brain in Stereotaxic Coordinates*. New York, NY: Academic Press. (2001).
42. Puelles L, Rubenstein JLR. A new scenario of hypothalamic organization: Rationale of new hypotheses introduced in the updated prosomeric model. *Front Neuroanat.* (2015) 9:27. doi: 10.3389/fnana.2015.00027
43. Toledano-Díaz A, Álvarez MI, Rodríguez JJ, Badiola JJ, Monzón M, Toledano A. Reflections on cerebellar neuropathology in classical scrapie. *Biomolecules.* (2021) 11:649. doi: 10.3390/biom11050649
44. Baizer JS. Unique features of the human brainstem and cerebellum. *Front Hum Neurosci.* (2014) 8:1–17. doi: 10.3389/fnhum.2014.00202
45. Galinsky R, Davidson JO, Lear CA, Bennet L, Green CR, Gunn AJ. Connexin hemichannel blockade improves survival of striatal GABA-ergic neurons after global cerebral ischaemia in term-equivalent fetal sheep. *Sci Rep.* (2017) 7:1–11. doi: 10.1038/s41598-017-06683-1
46. Gantert M, Kreczmanski P, Kuypers E, Jellema R, Strackx E, Bastian N, et al. Effects of in utero endotoxemia on the ovine fetal brain: a model for schizophrenia? *Front Biosci.* (2012) 4E:2745–53. doi: 10.2741/e588
47. D Isaacson, J L Mueller JCN and SS, Article R. Location and connectivity determine GABAergic interneuron survival in the brains of South Hampshire sheep with CLN6 neuronal ceroid lipofuscinosis. *Neurobiol Disorders.* (2008) 32:50–61. doi: 10.1016/j.nbd.2008.06.004.Location
48. Arciszewski MB, Calka J, Wasowicz K MM. Distribution and chemical coding of calretinin- and calbindin-expressing enteric neurons in the duodenum of the sheep. *Pol J Vet Sci.* (2009) 12:423–31.
49. Luo QQ, Hou Y, Yin N, Zhang HQ. Expression of kisspeptin/kiss1r system in developing hypothalamus of female rat and the possible effects on reproduction development and maintenance. *J Chin Med Assoc.* (2016) 79:546–53. doi: 10.1016/j.jcma.2016.01.019
50. Oliet SHR, Bonfardin VDJ. Morphological plasticity of the rat supraoptic nucleus - cellular consequences. *Eur J Neurosci.* (2010) 32:1989–94. doi: 10.1111/j.1460-9568.2010.07514.x

51. Wang SC, Parpura V, Wang YF. Astroglial regulation of magnocellular neuroendocrine cell activities in the supraoptic nucleus. *Neurochem Res.* (2021) 46:2586–600. doi: 10.1007/s11064-020-03172-2
52. Łapot M, Ciechanowska M, Malewski T, Mateusiak K, Misztal T, Przekop F. Changes in the GnRH mRNA and GnRH receptor (GnRH-R) mRNA levels in the hypothalamic-anterior pituitary unit of anestrus ewes after infusion of GnRH into the third cerebral ventricle. *Reprod Biol.* (2008) 8:149–61. doi: 10.1016/S1642-431X(12)60010-2
53. Pernia M, Díaz I, Colmenárez-Raga AC, Rivadulla C, Cudeiro J, Plaza I, et al. Cross-modal reaction of auditory and visual cortices after long-term bilateral hearing deprivation in the rat. *Brain Struct Function.* (2020) 225:129–48. doi: 10.1007/s00429-019-01991-w
54. Itiekey TL, Spear PD. Retinogeniculate projections in hooded and albino rats: an autoradiographic study. *Exp Brain Res.* (1976) 24:523–9.
55. Morin LP, Blanchard J, Moore ARY. Intergeniculate leaflet and suprachiasmatic nucleus organization and connections in the golden hamster. *Visual Neurosciences.* (1992) 8:219–23.
56. Jones EG. Synchrony in the interconnected circuitry of the thalamus and cerebral cortex. *Annal Acad Sci.* (2009) 1157:10–23. doi: 10.1111/j.1749-6632.2009.04534.x
57. Fiuza FP, Aquino ACQ, Câmara DA, Cavalcanti JRLP, Nascimento Júnior ES, Lima RH, et al. Region-specific glial hyperplasia and neuronal stability of rat lateral geniculate nucleus during aging. *Exp Gerontol.* (2017) 100:91–9. doi: 10.1016/j.exger.2017.11.001
58. Chronwall BM. Anatomy and physiology of the neuroendocrine arcuate nucleus. *Peptides.* (1985) 6:1–11. doi: 10.1016/0196-9781(85)90128-7
59. Cheng G, Coolen LM, Padmanabhan V, Goodman RL, Lehman MN. The kisspeptin/neurokinin B/dynorphin (KNDy) cell population of the arcuate nucleus: Sex differences and effects of prenatal testosterone in sheep. *Endocrinology.* (2010) 151:301–11. doi: 10.1210/en.2009-0541
60. Ciechanowska M, Łapot M, Antkowiak B, Mateusiak K, Paruszevska E, Malewski T, et al. Effect of short-term and prolonged stress on the biosynthesis of gonadotrophin-releasing hormone (GnRH) and GnRH receptor (GnRHR) in the hypothalamus and GnRHR in the pituitary of ewes during various physiological states. *Anim Reprod Sci.* (2016) 174:65–72. doi: 10.1016/j.anireprosci.2016.09.006
61. Amstalden M, Coolen LM, Hemmerle AM, Billings HJ, Connors JM, Goodman RL, et al. Neurokinin 3 receptor immunoreactivity in the septal region, preoptic area and hypothalamus of the female sheep: co-localisation in neurokinin B cells of the arcuate nucleus but not in gonadotrophin-releasing hormone neurones. *J Neuroendocrinol.* (2010) 22:1–12. doi: 10.1111/j.1365-2826.2009.01930.x
62. Ciechanowska M, Łapot M, Paruszevska E, Radawiec W, Przekop F. The influence of dopaminergic system inhibition on biosynthesis of gonadotrophin-releasing hormone (GnRH) and GnRH receptor in anoestrous sheep; Hierarchical role of kisspeptin and RFamide-related peptide-3 (RFRP-3). *Reprod Fertil Dev.* (2018) 30:672–80. doi: 10.1071/RD16309
63. Thankachan S, Rusak B. Juxtacellular recording/labeling analysis of physiological and anatomical characteristics of rat intergeniculate leaflet neurons. *J Neurosci.* (2005) 25:9195–204. doi: 10.1523/JNEUROSCI.2672-05.2005
64. Cassone VM, Speth JC, Card JP, Moore RY. Comparative anatomy of the mammalian hypothalamic suprachiasmatic nucleus. *J Biol Rhythms.* (1988) 3:71–91.
65. Garcia-Segura LM, Lorenz B, DonCarlos LL. The role of glia in the hypothalamus: Implications for gonadal steroid feedback and reproductive neuroendocrine output. *Reproduction.* (2008) 135:419–29. doi: 10.1530/REP-07-0540
66. Sharif A, Baroncini M, Prevot V. Role of glia in the regulation of gonadotropin-releasing hormone neuronal activity and secretion. *Neuroendocrinology.* (2013) 98:1–15. doi: 10.1159/000351867
67. Spergel DJ. Modulation of gonadotropin-releasing hormone neuron activity and secretion in mice by non-peptide neurotransmitters, gasotransmitters, and gliotransmitters. *Front Endocrinol.* (2019) 10:329. doi: 10.3389/fendo.2019.00329
68. Adachi S, Fujioka H, Kakehashi C, Matsuwaki T, Nishihara M, Akema T. Possible involvement of microglia containing cyclooxygenase-1 in the accumulation of gonadotrophin-releasing hormone in the preoptic area in female rats. *J Neuroendocrinol.* (2009) 21:1029–37. doi: 10.1111/j.1365-2826.2009.01928.x
69. Langlet F. Tanycytes: A Gateway to the metabolic hypothalamus. *J Neuroendocrinol.* (2014) 26:753–60. doi: 10.1111/jne.12191
70. Banstola A, Reynolds JNJ. Mapping sheep to human brain: the need for a sheep brain atlas. *Front Vet Sci.* (2022) 9:961413. doi: 10.3389/fvets.2022.961413